Inorganic Chemistry

pubs.acs.org/IC

Article

A Ruthenium(II) Water Oxidation Catalyst Containing a pH-Responsive Ligand Framework

Fabian L. Huber,[§] Anna M. Wernbacher,[§] Daniel Perleth, Djawed Nauroozi, Leticia González,* and Sven Rau*

Cite This: *Inorg. Chem.* 2021, 60, 13299−13308

Read Online

ACCESS | Metrics & More | Article Recommendations | Supporting Information

ABSTRACT: The synthesis of a new Ru^{II}-based water oxidation catalyst is presented, in which a nitrophenyl group is introduced into the backbone of dpp via a pH-sensitive imidazole bridge (dpp = 2,9-di-(2′-pyridyl)-1,10-phenanthroline). This modification had a pronounced effect on the photophysical properties and led to the appearance of a significant absorption band around 441 nm in the UV−vis spectrum upon formation of the monoprotonated species under neutral conditions. Theoretical investigations could show that the main contributions to this band arise from transitions involving the imidazole and nitrophenyl motif, allowing us to determine the pK_a value (6.8 ± 0.1) of the corresponding, twofold protonated conjugated acid. In contrast, the influence of the nitrophenyl group on the electrochemical properties of the catalytic center was negligible. Likewise, the catalytic performance of Ru(dppip-NO_2) and its parent complex Ru(dpp) was comparable over the entire investigated pH range (dppip-NO_2 = 2-(4-nitrophenyl)-6,9-di(pyridin-2-yl)-1*H*-imidazo[4,5-*f*][1,10]phenanthroline). This allowed the original catalytic properties to be retained while additionally featuring a functionalized ligand scaffold, which provides further modification opportunities as well as the ability to report the pH of the catalytic solution via UV−vis spectroscopy.

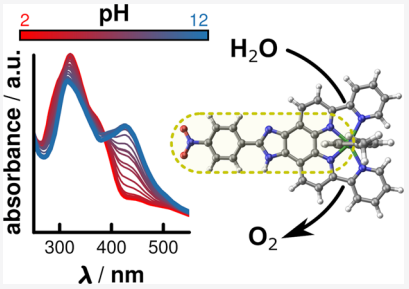

INTRODUCTION

Today, the demand for energy is mainly met by fossil fuels, which has a profound impact on climate change. An attractive option to address these challenges is the use of solar radiation as a sustainable energy source, especially since the amount of sunlight that strikes the earth within only 1 h (4.3×10^{20} J) is greater than the earth's energy consumption in a year (4.1×10^{20} J in 2001).[1] By converting solar energy into chemical energy via artificial photosynthesis, the energy is stored in the form of chemical bonds and can be released when needed.[2,3] A common example is the production of hydrogen as an energy carrier by splitting water into O_2 and H_2 (eq 1).

$$2H_2O \rightarrow O_2 + 2H_2 \quad (1)$$

This process can be subdivided into two half reactions. In the first half reaction, water is oxidized to dioxygen affording protons and electrons (eq 2). On the other hand, the second half reaction corresponds to the formation of two equivalents of dihydrogen by combining the protons and electrons produced in the first half reaction (eq 3).

$$2H_2O \rightarrow O_2 + 4H^+ + 4e^- \quad (2)$$

$$4H^+ + 4e^- \rightarrow 2H_2 \quad (3)$$

Due to the high activation barrier of four proton-coupled electron transfers (PCETs) and the endothermicity of the oxygen−oxygen bond formation, the oxidation of water is considered to be the bottleneck of water splitting.[4−7] Metal complexes, especially systems based on ruthenium, have attracted considerable interest as active catalysts for water oxidation.[8−10] In addition, such molecular water oxidation catalysts (WOCs) can be modified via the introduction of different functional groups into the ligand framework. Such modifications, however, usually have a strong influence on the redox properties of the catalyst, which in some cases might not be desirable.

One established example is $[Ru(dpp)(pic)_2](PF_6)_2$ (Ru-(dpp); dpp = 2,9-di-(2′-pyridyl)-1,10-phenanthroline; pic = 4-picoline), originally published by Thummel *et al.*[11,12] The redox properties of this complex were especially susceptible to modifications of the axial ligands. However, converting the dpp backbone to a phenazine derivative (dppdppz = 3,6-di-(pyrid-2′-yl)-dipyrido[3,2-*a*:2′,3′-*c*]phenazine) had only a minor impact on the catalytic performance.[13] We were therefore interested whether it would be possible to introduce alternative functional groups at the dpp backbone, which could serve as a starting point for further modifications. Furthermore, we

Received: June 1, 2021
Published: August 10, 2021

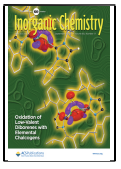

wanted to explore if such modifications retained the innocent character with respect to the catalytic performance. As functionalization of highly substituted phenanthrolines requires a facile access, we utilized the literature-known quinone moiety of dpp for the formation of an imidazolyl moiety. To this end, a nitrophenyl group was introduced via a pH-sensitive imidazole bridge, thereby giving access to $[Ru(dppip\text{-}NO_2)(pic)_2](PF_6)_2$ ($Ru(dppip\text{-}NO_2)$, dppip-NO_2 = 2-(4-nitrophenyl)-6,9-di(pyridin-2-yl)-1*H*-imidazo[4,5-*f*][1,10]-phenanthroline (Figure 1).

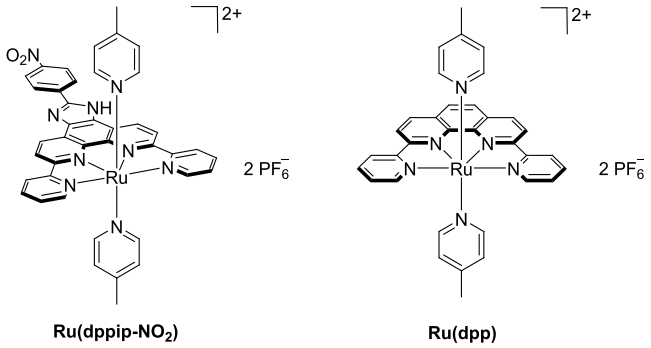

Figure 1. Structure of $Ru(dppip\text{-}NO_2)$ and Ru(dpp).

In the present report, we describe the synthesis of $Ru(dppip\text{-}NO_2)$ and its photophysical and preliminary electrochemical characterization, along with theoretical studies and first photocatalytical water oxidation experiments. We address the questions of how the photophysical properties of the new Ru complex are affected by (i) the chemical modification of the dpp-based acceptor ligand and (ii) the protonation state of the imidazole moiety of dppip-NO_2. Because the interpretation of the experimental data proved to be difficult, quantum chemical methods were used to complement the experimental spectroscopic studies and to provide insight into the nature of the electronic excitations. Furthermore, pH-dependent light-driven catalytic runs were performed to investigate the influence of the degree of protonation of the ligand scaffold, i.e., of the amphoteric imidazole moiety, on the catalytic behavior of the WOC.

RESULTS AND DISCUSSION

Synthesis and Structural Characterization. The free ligand dppip-NO_2 was obtained via a microwave-assisted Debus−Radziszewski reaction of $dppO_2$ with 4-nitrobenzaldehyde and ammonium acetate in glacial acetic acid following literature-known procedures (Scheme 1).[14,15] To prevent solvation of imidazolium cations, it was crucial that the reaction mixture was neutralized with diluted ammonia (25%). This reaction resulted in a good yield of 85%, and the ligand was characterized via ^{1}H NMR spectroscopy (Figure S3), while ^{13}C NMR measurements were not possible due to low solubility. The constitution of dppip-NO_2 was further confirmed by high-resolution mass spectrometry (HRMS; Figure S7).

The synthesis of the complex $Ru(dppip\text{-}NO_2)$ followed a modified literature procedure.[12] Purification of the complex was obtained by washing with water and diethyl ether followed by diffusion crystallization (DMF/Et_2O), resulting in a moderate yield of 29% of pure $Ru(dppip\text{-}NO_2)$.

The formation of the desired product could be confirmed by ^{1}H NMR (Figure S5) and HRMS (Figures S8 and S9). Analysis of H,H-COSY experiments further allowed the assignment of proton signals (Figure S6). Due to the amphoteric behavior of the imidazole unit,[16] the corresponding proton was not detected via NMR spectroscopy, resulting in a pseudo C_{2v}-symmetry for both the complex $Ru(dppip\text{-}NO_2)$ and the free ligand dppip-NO_2. Characterization via ^{13}C NMR spectroscopy was not possible because of a relatively poor solubility of the complex.

Since no experimental crystal structure of $Ru(dppip\text{-}NO_2)$ could be produced so far, theoretical methods were used to gain insight into its structure. The suitability of the computational approach to describe such Ru complexes is justified by the good agreement that was obtained between the computed structure of Ru(dpp) and its experimental crystal structure.[12,13] We therefore employed the same methodology

Scheme 1. Synthesis Route toward $Ru(dppip\text{-}NO_2)$

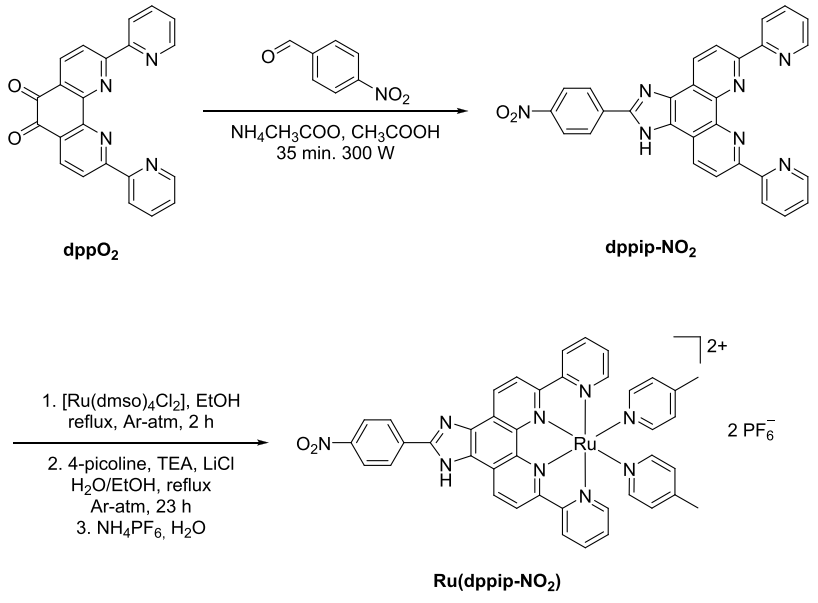

https://doi.org/10.1021/acs.inorgchem.1c01646
Inorg. Chem. 2021, 60, 13299−13308

to investigate Ru(dppip-NO_2), which was found to exhibit a similar structure like Ru(dpp). In particular, the coordination sphere of the Ru center is hardly affected by the modified equatorial dppip-NO_2 ligand. The dpp or dppip-NO_2 ligand binds with four N atoms to Ru exhibiting two short Ru−N bonds to the central phenanthroline ring (1.96 Å) and two elongated Ru−N bonds of about 2.18−2.19 Å to the peripheral pyridine substituents of the equatorial ligand. The rather large N−Ru−N bond angle of these peripheral pyridines of 125−126° (compared to 90° in an ideal octahedral geometry) and long Ru−N bond lengths were suggested to facilitate an attack of water in the case of Ru(dpp).[13,17]

Due to the featured imidazole motif of Ru(dppip-NO_2), the structure of the complex depends on the degree of protonation of the imidazole moiety. To investigate this dependency, structures with a double-protonated (2H-Ru(dppip-NO_2)) and deprotonated imidazole group (0H-Ru(dppip-NO_2)) were calculated in addition to the parent complex 1H-Ru(dppip-NO_2), as indicated in Figure 2. Interestingly, the nitrophenyl

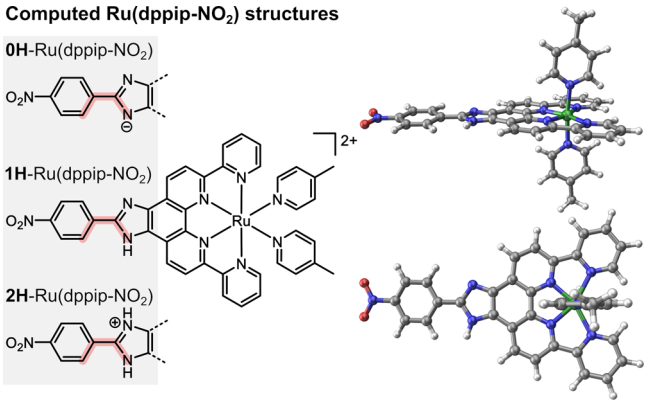

Figure 2. Computed Ru(dppip-NO_2) structures with the deprotonated imidazole moiety (0H-Ru(dppip-NO_2)), with one proton (1H-Ru(dppip-NO_2)), and with two protons on the imidazole (im) group (2H-Ru(dppip-NO_2)). The nitrophenyl dihedral angle with respect to the im-dpp ring system is highlighted in red. The geometry of 1H-Ru(dppip-NO_2) is shown on the right (side view and top view).

group of dppip-NO_2 is slightly rotated with respect to the imidazole-dpp ring system, depending on the degree of protonation. Specifically, the nitrophenyl dihedral angle, highlighted in red in Figure 2, increases with the number of protons/H-atoms on the imidazole group in the following order, probably due to steric effects: 0H-Ru(dppip-NO_2) (nearly planar, −0.8°) < 1H-Ru(dppip-NO_2) (−5°) < 2H-Ru(dppip-NO_2) (−25°) (cf. Figure 3c, see also Figure S10 and Table S1).

Photophysical Properties. To characterize the new Ru(dppip-NO_2) complex and to better understand its difference from Ru(dpp), UV−vis spectra of both complexes were recorded. It is very surprising to note that the new complex Ru(dppip-NO_2) shows a very intense orange-red color once dissolved in acetonitrile. The recorded UV−vis spectra show a maximum at 441 nm. This feature is completely absent in the parent compound Ru(dpp) under identical conditions. Addition of base and acid to these probes shows that, for Ru(dppip-NO_2), absorption bands change in intensity and energy, whereas no such behavior could be observed for Ru(dpp). As this interesting and unexpected behavior could not be understood from a purely experimental perspective, more detailed investigations have been performed. Thus, in the following, the results of the photophysical and theoretical investigations will be described together.

Electronic Structure. Figure 3a shows the computed energetic order of the frontier molecular orbitals (MOs) of 1H-Ru(dppip-NO_2) and its (de)protonated forms compared to Ru(dpp). The gap between the highest occupied MO (HOMO) and lowest unoccupied MO (LUMO) decreases from 3.1 eV in Ru(dpp) to 2.8 eV in 1H-Ru(dppip-NO_2) and ca. 2.7 eV in the (de)protonated complexes. In addition, the HOMO-3 and LUMO of Ru(dpp) and of 0H,1H,2H-Ru(dppip-NO_2) are depicted as they are involved in the electronic excited states underlying the UV−vis absorption spectra (see below in the next section). While the HOMO−LUMO gap in 0H,1H,2H-Ru(dppip-NO_2) remains similar, the energy of the HOMO-3 decreases with the number of protons on dppip-NO_2, thus increasing the LUMO−HOMO-3 gap (Figure 3b). Other relevant highest occupied and lowest unoccupied MOs can be found in Figure S11.

In both Ru(dpp) and (1H),2H-Ru(dppip-NO_2), the first three d_{Ru}-based HOMOs, which are shaded in gray in Figure 3a, are nearly degenerate. The HOMO of 1H-Ru(dppip-NO_2) also has a contribution from the dppi ligand, but the d_{Ru} character is still dominant. In contrast, the planar 0H-Ru(dppip-NO_2) complex exhibits a HOMO of $d_{Ru}/\pi_{im\text{-}dpp}$ character, which is slightly higher in energy than the d_{Ru}-based HOMO-1,2. The $d_{Ru}/\pi_{im\text{-}dpp\text{-}(ph)}$ HOMO-3 already exhibits a contribution of the imidazole group and to a lesser extent of the phenyl ring (ph) in 1H-Ru(dppip-NO_2) as well as in its (de)protonated forms.

A major difference between Ru(dpp) and Ru(dppip-NO_2) becomes apparent in the LUMO, which is centered on the nitrophenyl group in the latter complex ($\pi^*_{nitrophenyl}$). The subsequent higher-lying unoccupied MOs as well as the LUMO in Ru(dpp) are of π^*_{dpp} character in all complexes. The LUMO+3 in Ru(dpp), LUMO+4 in 0H,1H-Ru(dppip-NO_2), and LUMO+5 in 2H-Ru(dppip-NO_2) are of π^*_{pic} character.

Based on these reference points, detailed investigations were performed. Figure 4 compares the experimental UV−vis spectra of Ru(dpp) recorded in acetonitrile (MeCN), Ru(dppip-NO_2) in MeCN/triethylamine (TEA, 0H,1H-Ru-(dppip-NO_2)), and MeCN/trifluoroacetic acid (TFA, protonated 2H-Ru(dppip-NO_2)) with the computed spectra in MeCN (convoluted spectra based on the corresponding equilibrium geometries in blue). In addition, a UV−vis titration of Ru(dppip-NO_2) in 80 vol-% Britton−Robinson buffer and 20 vol-% MeCN was performed (Figure 4) and the computed spectra of the protonated and deprotonated complexes are compared to the experimental spectra of the titration at pH values of 1.95 and of 12.15, respectively.

The excited states were first characterized by inspection of the natural transition orbitals (NTOs). NTO pairs of states contributing to the strong absorption band in the visible region in 2H,1H,0H-Ru(dppip-NO_2) are shown in Figure 4 on the right. Furthermore, an automatized analysis of the transition density matrix was performed with TheoDORE,[18−20] enabling a classification of the states in terms of their charge transfer character.[21] The states can be labeled as locally excited ligand-centered (LC) states or charge transfer excitations, e.g., metal-to-ligand charge transfer (MLCT) or ligand-to-ligand charge transfer (LLCT). Ligand-to-metal charge transfer (LMCT) excitations and metal centered Ru d−d excitations were not

https://doi.org/10.1021/acs.inorgchem.1c01646
Inorg. Chem. 2021, 60, 13299−13308

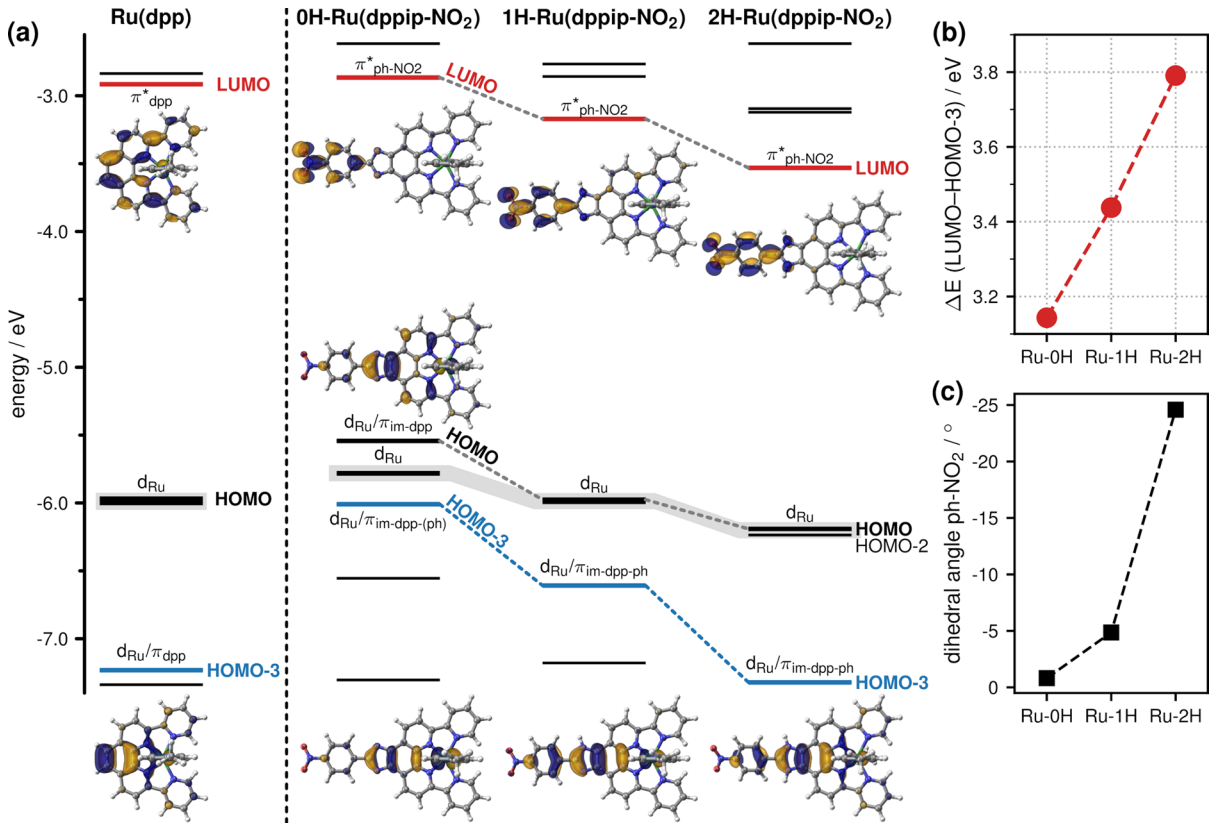

Figure 3. (a) Calculated energetic order of frontier molecular orbitals (MOs) of 0H,1H,2H-Ru(dppip-NO_2); d_{Ru} orbitals are shaded in gray, and the HOMO-3 and LUMO are highlighted in blue and red, respectively. (b) LUMO−HOMO-3 gap. (c) Dihedral angles of the nitrophenyl group with respect to the im-dpp ring system.

found to be important for the absorption spectra of these Ru complexes.

The most prominent difference in the spectra of Ru(dpp) and Ru(dppip-NO_2) is the strong absorption band of the latter in the visible energy range, which is not observed in Ru(dpp). Here, 1H-Ru(dppip-NO_2) features a state of high intensity, the S_{11} at 421 nm (2.9 eV), which is due to an excitation to the nitrophenyl group, as can be seen in the NTO pairs shown in Figure 4 on the right. S_{11} mostly corresponds to a $d_{Ru}/\pi_{im\text{-}dpp\text{-}ph} \rightarrow \pi^*_{nitrophenyl}$ LLCT/MLCT excitation with a contribution of a $d_{Ru} \rightarrow \pi^*_{dpp,NO2}$ MLCT excitation. As shown in Figure S13, a decomposed spectrum of 1H-Ru(dppip-NO_2) taking only states without a significant contribution of the nitrophenyl group into account closely resembles the spectrum of Ru(dpp). The differences from Ru(dpp) in the visible energy range seem to be a consequence of transitions to the nitrophenyl-centered LUMO in 1H-Ru(dppip-NO_2).

Moreover, the absorption band of Ru(dppip-NO_2) in the visible energy range, which is highlighted by the gray bars in Figure 4, is pH-dependent. The calculated band maximum shifts to higher energies with increasing number of protons in the order of 2H-Ru(dppip-NO_2) 394 nm < 1H-Ru(dppip-NO_2) 419 nm < 0H-Ru(dppip-NO_2) 458 nm, while the character of the involved states stays similar (cf. NTOs in Figure 4 and Table S2). In all complexes, they can be described by a $d_{Ru}/\pi_{im\text{-}dpp\text{-}ph} \rightarrow \pi^*_{nitrophenyl}$ excitation (mostly HOMO-3 → LUMO), where the d_{Ru} contribution decreases and the contribution of the phenyl ring increases with increasing number of protons. Both 1H-Ru(dppip-NO_2) and 0H-Ru(dppip-NO_2) exhibit an additional Ru/(dppi) → dpp MLCT contribution, which increases the overall MLCT character of the absorption band. In 0H-Ru(dppip-NO_2), another intense state (S_{12}) contributes to the band in the visible region, which is predominantly of $d_{Ru} \rightarrow \pi^*_{dpp}$ MLCT character. The shift of vis states S_{10}, S_{11}, and S_{13} of 0H,1H,2H-Ru(dppip-NO_2) to higher energies correlates with an increase in the LUMO−HOMO-3 gap (see Figure 3b). Considering that these states consist of predominantly HOMO-3 → LUMO character in all complexes, this correlation suggests that the stabilization of the HOMO-3 with increasingly positive charge on the imidazole group contributes to the increase in excitation energy in the order of 0H-Ru(dppip-NO_2) < 1H-Ru(dppip-NO_2) < 2H-Ru(dppip-NO_2). A similar blue shift of the vis band upon protonation was reported for a Ru complex bearing a 2,2′-biimidazole ligand, which was also attributed to a stabilization of d_{Ru}/π orbitals that contribute to the electronic excitation.[22]

Like Ru(dpp), Ru(dppip-NO_2) is not emissive in MeCN and CH_2Cl_2 at room temperature.[12,13] A likely explanation for the absence of any appreciable emission is the highly distorted coordination geometry between the tetradentate dpp-sphere and the ruthenium center, which lowers the d−d states and allows for non-radiative relaxation of the excited state.[12,13] Similar conclusions have been drawn for the negligible emission at room temperature of $[Ru(tpy)_2]^{2+}$.[23,24]

pK_a Determination. As briefly discussed above, the pH value of the surrounding solution significantly influences the photophysical properties of Ru(dppip-NO_2). During the course of titration experiments, a rising band at 425.5 nm and a decreasing intensity for the band at 320.5 nm upon

https://doi.org/10.1021/acs.inorgchem.1c01646
Inorg. Chem. 2021, 60, 13299−13308

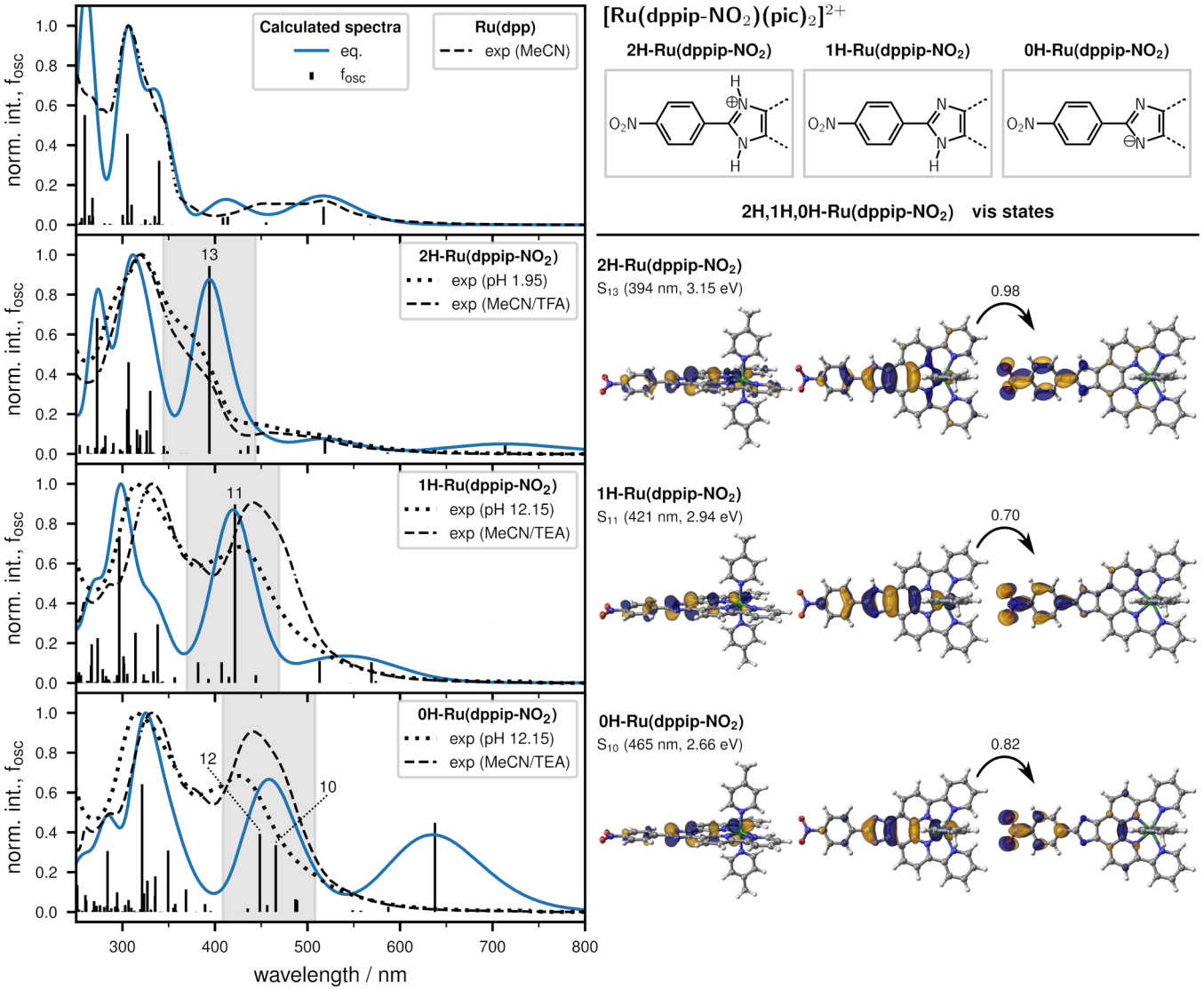

Figure 4. Calculated UV−vis absorption spectra of Ru(dpp) and 2H,1H,0H-Ru(dppip-NO_2) equilibrium geometries in MeCN, and oscillator strengths f_{osc} compared to the experimental spectra of Ru(dpp) in MeCN and Ru(dppip-NO_2) in MeCN/TFA, MeCN/TEA (dashed line), and Britton−Robinson buffer/MeCN (dotted line). For the calculated spectra of the equilibrium geometries, Gaussian functions with a full width at half-maximum fwhm of 0.35 eV were used. No shifting has been applied. The natural transition orbitals of the intense vis states of 2H,1H,0H-Ru(dppip-NO_2) are shown on the right, and the structures with two, one, or zero protons on the imidazole group of the dppip-NO_2 ligand are indicated at the top. (B3LYP-D3BJ, ZORA, ZORA-def2-TZVP, and ZORA-TZVP on Ru, C-PCM (MeCN)).

increasing the pH were observed, along with the formation of an isosbestic point at 384 nm. These spectral changes in absorption bands at 320.5 and 425.5 nm could be used to determine the pK_a value of Ru(dppip-NO_2) by using a sigmoidal fit on the titration curves, which yield inflection points at p$K_a^{320.5}$ = 7.06 ± 0.07 and p$K_a^{425.5}$ = 6.59 ± 0.05 (Figure S14).[22,25,26] Based on these two values, a pK_a of 6.8 ± 0.1 was determined, which likely corresponds to the twofold protonated form of the imidazole motif (2H-Ru(dppip-NO_2)), as other imidazoles have similar pK_a values for their respective conjugated acids.[27] Likewise, the pK_a corresponding to the mono-protonated imidazole motif was expected to be around 12−14,[27] and the exact value however could not be determined as the addition of additional NaOH resulted in phase separation between MeCN and the aqueous buffer solution as well as partial precipitation of Ru(dppip-NO_2).

A dependence of the vis absorption band on the protonation state of the imidazole group is also shown by computing pH-dependent spectra using the spectra of 2H-Ru(dppip-NO_2) and 1H-Ru(dppip-NO_2) and scaling their intensities based on an experimental pK_a of 6.8. To account for vibrational effects, the spectra of 2H,1H,0H-Ru(dppip-NO_2) were calculated using 50 geometries for each Ru complex sampled from a temperature-dependent Wigner distribution at 300 K. Figure 5 compares the computed pH-dependent spectra with the experimental spectra of Ru(dppip-NO_2) in Britton−Robinson buffer/MeCN.

A good agreement is obtained between the spectra calculated in this way and the pH-dependent experiments. The increase in intensity in the visible energy range with increasing pH is clearly shown, which is due to the dppip-NO_2-dominated band of 1H-Ru(dppip-NO_2) at 429 nm and lower energies in the calculated spectrum. The absorption band maximum of the protonated complex 2H-Ru(dppip-NO_2), on the other hand, is only observed in the UV range at 329 nm. In contrast, the B3LYP spectra suggest that the deprotonated

https://doi.org/10.1021/acs.inorgchem.1c01646
Inorg. Chem. 2021, 60, 13299−13308

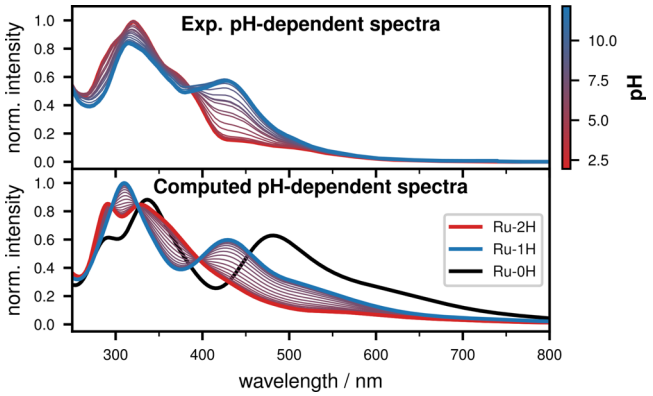

Figure 5. Experimental pH-dependent UV−vis spectra of Ru(dppip-NO_2) in Britton−Robinson buffer/MeCN (top) and computed pH-dependent spectra (bottom). For the latter, the Wigner spectra of 2H,1H-Ru(dppip-NO_2) were used and their intensities scaled based on an experimental pK_a of 6.8. In addition, the Wigner spectrum calculated for 0H-Ru(dppip-NO_2) is shown in black. (B3LYP-D3BJ, ZORA, ZORA-def2-TZVP, and ZORA-TZVP on Ru, C-PCM (MeCN)).

complex 0H-Ru(dppip-NO_2) shows an intense band at rather low energies (481 nm, black spectrum). This might indicate that it does not contribute significantly to the experimental pH-dependent spectra in the investigated pH range. The deprotonated complex was hence not considered in the computed pH-dependent spectra. The changes in the absorption band are mainly caused by the shift of the excitation energy of the intense states in the visible energy range to higher energies with increasing number of protons on the dppip-NO_2 ligand.

Electrochemistry. The electrochemical features of Ru(dppip-NO_2) were investigated by cyclic voltammetry in 0.1 M solution of nBu$_4$NPF$_6$ in DMF using a glassy carbon working electrode, a silver reference electrode, and a Pt-wire as the counter electrode. Potentials were referenced against ferrocene/ferricenium (Fc/Fc^+) (Figure S15). The pertinent data is summarized in Table 1.

Table 1. Electrochemical Potentials E vs Fc/Fc^+ [V] for Ru(dppip-NO_2), dppip-NO_2, and Ru(dpp)

	E_{ox}	E_{red1}	E_{red2}	E_{red3}	E_{red4}
Ru(dppip-NO_2)	0.64	−1.07	−1.24	−1.49	−1.79
dppip-NO_2		−1.03	−1.35	−1.65	
Ru(dpp)	0.67	−1.42	−1.65		

In the anodic region, Ru(dppip-NO_2) showed a quasi-reversible oxidation at 0.64 V, which can likely be assigned to the first oxidation of the ruthenium center (Ru(II/III)). In the cathodic region, the complex featured multiple irreversible reductions around −1.07, −1.24, −1.49, and −1.79 V. These redox events presumably are ligand-based as suggested by a comparison with the electrochemical features of dppip-NO_2 showing irreversible reduction processes at −1.03, −1.35, and −1.65 V (Figure S16). Interestingly, the introduction of the imidazole moiety at the periphery of the phenanthroline seems not to impact the redox properties of the catalytic center significantly as only a slight cathodic shift of −0.03 V is observed for the oxidation of Ru(II/III) in Ru(dpp). It is worth noting that Ru(dppip-NO_2) suffers degradation upon electrochemical cycling as observed in new features between −0.7, 0.3, and 0.52 V (Figure S16).

Photocatalytical Water Oxidation. For light-driven water oxidation, a three-component system was investigated consisting of the catalyst Ru(dppip-NO_2) (2.6 μM), the photosensitizer [Ru(dceb)$_2$(bpy)](PF$_6$)$_2$ (0.3 M, PS, dceb = diethyl[2,2′-bipyridine]-4,4′-dicarboxylate), and $Na_2S_2O_8$ (10 mM) as the sacrificial agent in aqueous H_3BO_3/$NaHCO_3$ buffer (5 mL, 0.08 M H_3BO_3 containing 0.2 mL of MeCN to improve solubility). The catalytic runs were carried out in sealed glass vessels equipped with two oxygen sensor spots, which allowed for independent measurement of the oxygen concentration in the gas and the liquid phase;[28] further, the samples were stirred constantly during the whole run.

Figure 6a depicts a catalytic run of Ru(dppip-NO_2) conducted at pH 6.07, where the oxygen concentrations of the individual phases (liquid and gas) are measured and the total TON (turnover number) is calculated from those measurements.

As shown in Figure 6a, the overall O_2 concentration rose rapidly upon irradiation and reached a plateau after *ca.* 8 min, reaching a total TON (liquid + gas phase) of *ca.* 168. In the liquid phase, O_2 concentration reached its maximum after *ca.* 6 min, after which the O_2 concentration decreases steadily. The reason behind this is that dissolved O_2 slowly diffuses from the liquid into the gas phase. After 6 min, this diffusion proceeds faster than the generation of new O_2, indicating that a decrease in catalytic activity below 0.5 s^{-1} under the utilized conditions results in net loss of O_2 from the liquid phase.[28] The overall decrease in catalytic activity becomes more evident by analyzing the development of the TOF (turnover frequency) over the course of the catalytic run (Figure 6b). The maximum TOF of 0.9 s^{-1} was reached in 1 min, corresponding to the initial rapid increase in O_2, after which the catalytic activity decreases asymptotically, only reaching a TOF of 0.3 s^{-1} after 10 min.

However, to determine ideal conditions for the photocatalytic water splitting, water oxidation experiments have been performed at different pH values in a pH screening process. The pH value was adjusted by adding different amounts of solid $NaHCO_3$ to the aqueous 0.08 M H_3BO_3 solution, thereby creating several borate buffers of different pH values. During this screening, the catalytic activity was determined for each pH value three times and the average TON and TOF were calculated. For reference, the same procedure was applied using Ru(dpp) as the catalyst. Figure 7 summarizes the results of the pH screenings.

Compared to Ru(dpp), Ru(dppip-NO_2) consistently yields higher amounts of O_2, with the exception of catalytic runs performed at pH 6.07, where Ru(dpp) reaches a TON of 193 ± 14 compared to 163 ± 31 of Ru(dppip-NO_2) (Figure 7c). Further, both complexes show the highest catalytic yield at pH 6.07. It is however worth noting that, within the margins of error, both catalysts show very comparable performances. The TOFs of both complexes also behave similarly; it should however be pointed out that Ru(dppip-NO_2) shows the highest activity at pH 6.73, reaching a TOF of *ca.* 1 s^{-1} (Figure 7a). This activity cannot be maintained for a long time. In contrast, at pH 6.07, a relatively high TOF can be maintained by both catalysts for a longer time, resulting in the highest TONs at pH 6.07.

These findings indicate no significant influence of the nitrophenyl group of the dppip-NO_2 ligand on the catalytic

https://doi.org/10.1021/acs.inorgchem.1c01646
Inorg. Chem. 2021, 60, 13299−13308

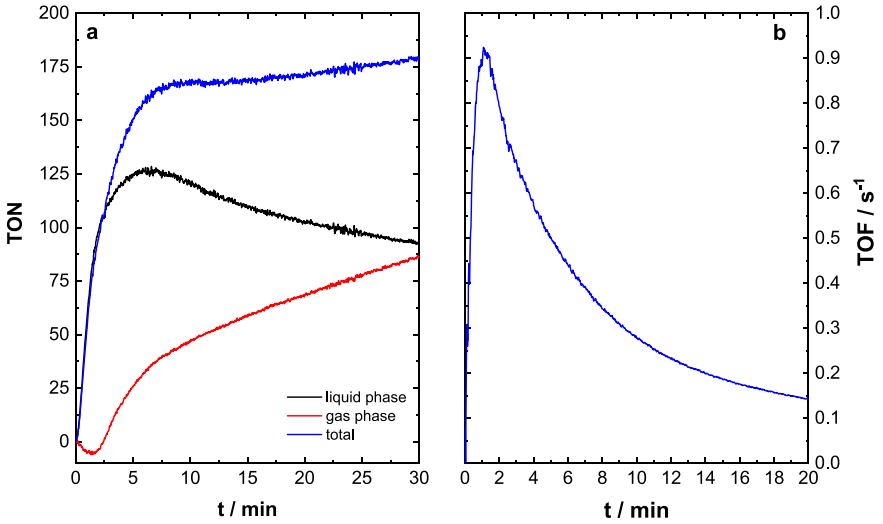

Figure 6. Representative catalytic run of Ru(dppip-NO_2) at pH 6.07. (a) TON as determined in the respective phases (liquid and gas) and the total TON (liquid + gas phase). (b) TOF (turnover frequency) development over the catalytic run based on the total TON. Conditions: Ru(dppip-NO_2), 2.6 μM; PS, 0.3 mM; and $Na_2S_2O_8$, 10 mM; solvent: 96 vol-% aqueous H_3BO_3/$NaHCO_3$ buffer (0.08 M H_3BO_3) and 4 vol-% MeCN. Irradiation with one LED stick, λ_{max} = 470 nm, ca. 50 mW cm^{-2}, continuous stirring during the reaction.

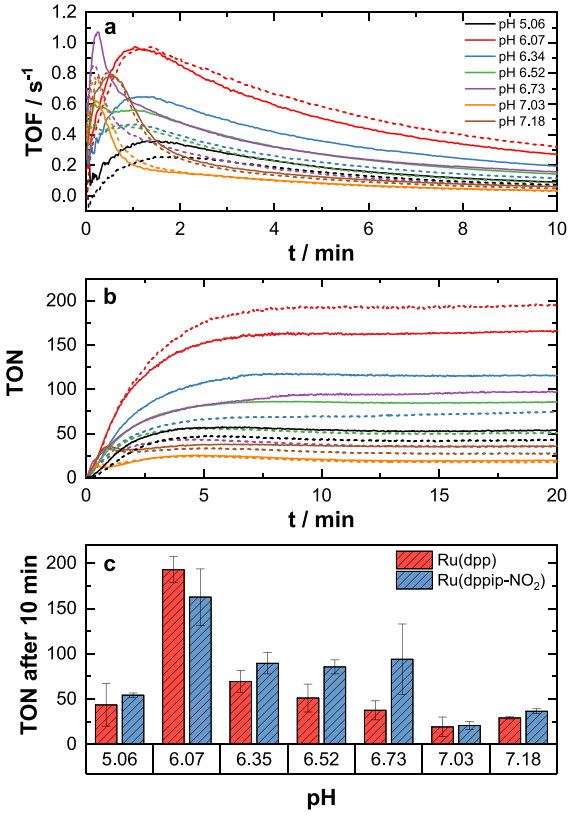

Figure 7. (a) Average total TOFs of the pH screening. (b) Average TONs of the pH screening. Results for Ru(dpp) are given in dotted lines, while solid lines refer to Ru(dppip-NO_2). (c) Comparison of the overall TONs after 10 min between Ru(dpp) and Ru(dppip-NO_2). Conditions: Ru(dppip-NO_2)/Ru(dpp), 2.6 μM; PS 0.3, mM; and $Na_2S_2O_8$, 10 mM; solvent: 96 vol-% aqueous H_3BO_3/$NaHCO_3$ buffer (0.08 M H_3BO_3) and 4 vol-% MeCN. Irradiation with one LED stick, λ_{max} = 470 nm, ca. 50 mW cm^{-2}, continuous stirring during the catalytic run.

Ru-center. At pH 6, a 2 e^-/2 H^+ process involving a water molecule from $[Ru^{II}]^{2+}$ to the seven-coordinated $[Ru^{IV}(O)]^{2+}$ was proposed as a possible initial oxidation step during catalysis for Ru(dpp).[29] Because of the similar activity and structure and the negligible influence of the nitrophenyl group, it is reasonable to assume an analogous mechanism for Ru(dppip-NO_2).

Nevertheless, it has also been suggested that, prior to active oxygen evolution, an oxygen atom transfer from Ru to the N-atoms of the outer pyridines may take place. This leads to the formation of a di-oxo species as the active catalyst displaying an O,N,N,O tetradentate ligand sphere.[30,31] To reveal whether, also for Ru(dppip-NO_2), such a species might represent an intermediate of the catalytic cycle, chemical oxidation of Ru(dppip-NO_2) using $(NH_4)_2[Ce(NO_3)_6]$ (CAN) according to a previous literature report was performed.[31] Mass spectrometry revealed that, by increasing the amount of added CAN, the signal assigned to Ru(dppip-NO_2) decreased and new peaks that can be assigned to $[M\text{-}2PF_6^- + O]^{2+}$ and $[M\text{-}2PF_6^- + 2O]^{2+}$ increased in intensity (see Figures S16–S19). Interestingly, by increasing the amount of added CAN from 8 to 12 equiv, peaks that were assigned to $[M\text{-}2PF_6^- + O]^{2+}$-derived species vanished and those of the $[M\text{-}2PF_6^- + 2O]^{2+}$ species increased. We thus conclude that, also for Ru(dppip-NO_2), a species containing an O,N,N,O coordination sphere may represent an important intermediate of the catalytic cycle.

CONCLUSIONS

A new dpp-based ligand scaffold and the corresponding WOC, Ru(dppip-NO_2), could be prepared by introducing a nitrophenyl group to the tetradentate ligand via a pH-sensitive imidazole bridge. This modification had a pronounced effect on the photophysical properties of the complex. Compared to the parent complex Ru(dpp), the new complex exhibits an intense absorption at 441 nm in the singly protonated form. The main contributions to this absorption band are transitions involving the imidazole and nitrophenyl motifs, as shown by TDDFT calculations. Consequently, due to the amphoteric nature of the imidazole group, this band was mostly affected by the change in the pH of the solution. It shifts to higher energies with increasing degree of protonation of dppip-NO_2,

https://doi.org/10.1021/acs.inorgchem.1c01646
Inorg. Chem. 2021, 60, 13299−13308

whereas the character of the transitions has not changed significantly. (De)protonation of the imidazole group also affects the dihedral angle between the nitrophenyl group and the imidazole−dpp ring system. However, the blue shift of the excitation energy seems to be an electrostatic effect related to the stabilization of the HOMO-3 with increasingly positive charge on the imidazole group.

In contrast to the changes in the photophysical properties, the redox potential of the Ru^{II}/Ru^{III}-wave of Ru(dppip-NO_2) is comparable to Ru(dpp), differing only by 0.03 V. Likewise, both WOCs show similar catalytic performance. Interestingly, this similar performance persisted throughout the investigated pH range, despite the pH-sensitive imidazole motif of Ru(dppip-NO_2) that possesses its pK_a value within the range of the investigated pH regime. Therefore, it can be concluded that the catalytic performance of the Ru-center was not significantly affected by the chemical modification of the dpp ligand despite the influence of the nitrophenyl group on the electronic states of the metal complex. Thus, the original catalytic properties of the parent complex were preserved. This observed independence of catalytic performance from the degree of protonation of the ligand is highly gratifying albeit not expected. Imidazole-based ligand structures in related complexes show a strong impact of the protonation state on the electronic states of the coordinated ruthenium centers.[32] Moreover, water oxidation catalysis with molecular catalysts usually shows a susceptibility of performance to different proton concentrations.[33,34] This holds especially true for the OEC in biological photosynthesis where ligand protonation states play a very important role in determining the overall catalytic activity.[35] Thus, Ru(dppip-NO_2) might serve as an active WOC capable of additionally reporting the local pH value in, e.g., polymeric materials.[36,37]

The present work can provide foundations for further developments in WOC systems. Ru(dppip-NO_2) could serve as a WOC building block and a starting point for further modifications, such as substitution of the nitro group for an amide or azide one, which in turn could be used in click-chemistry or Schiff's base reactions. At the same time, the presented modification strategy preserves the original catalytic properties, thus providing a WOC building block that offers a predictable catalytic behavior.

EXPERIMENTAL SECTION

2-(4-Nitrophenyl)-6,9-di(pyridin-2-yl)-1*H*-imidazo[4,5-*f*]-[1,10]phenanthroline (dppip-NO_2). The free ligand was synthesized according to a modified literature procedure.[15] A mixture of 154.5 mg of $dppO_2$ (0.42 mmol, 1 equiv), 80.9 mg of 4-nitrobenzaldehyde (0.54 mmol, 1.3 equiv), and 1.45 g of ammonium acetate (18.0 mmol, 44 equiv) was suspended in 15 mL of acetic acid. The suspension was refluxed in a microwave-assisted reaction (1.5 min 600 W, 35 min 300 W). Upon cooling to room temperature, a brown precipitate formed. After diluting the solution with 45 mL of water, the pH was adjusted to pH 8 using conc. ammonia solution. Filtering off the solid and washing it with water and diethyl ether and subsequently drying it under high vacuum conditions yielded 179 mg (0.36 mmol, 85%) of dppip-NO_2 as a brown-orange solid.

^{1}H NMR (DMSO, 400 MHz,): δ 9.03 (d, J = 8.4 Hz, 2H), 8.98 (d, J = 7.9 Hz, 2H), 8.88 (d, J = 8.5 Hz, 2H), 8.79 (d, J = 3.9 Hz, 2H), 8.52 (d, J = 8.9 Hz, 2H), 8.46 (d, J = 9.1 Hz, 2H), 8.14 (td, J = 7.7, 1.7 Hz, 2H), 7.60−7.53 (m, 2H). HRMS/ESI (+): calcd. for $C_{29}H_{18}N_7O_2$ 496.15165, found 496.15122 $[M + H]^+$.

[Ru(dppip-NO_2)(pic)$_2$](PF$_6$)$_2$ (Ru(dppip-NO_2)). The synthesis of Ru(dppip-NO_2) followed a modified literature synthesis.[12,13] In a 250 mL Schlenk flask, 100.6 mg of dppip-NO_2 (0.22 mmol, 1 equiv) and 138.2 mg of $[Ru(dmso)_4Cl_2]$ (0.29 mmol, 1.3 equiv) were suspended in 75 mL of EtOH and de-aerated for 2 h using argon. The degassed suspension was refluxed under inert conditions for 2 h before a degassed aqueous (20 mL of H_2O) solution of 547.7 mg of LiCl (12.9 mmol, 59.8 equiv), 1.3 mL of TEA (9.3 mmol, 43.2 equiv), and 1.26 mL of 4-picoline (12.9 mmol, 43.2 equiv) was added. The resulting mixture was further refluxed under an argon atmosphere for 23 h. The obtained dark red solution was concentrated via a rotary evaporator, and the crude product was precipitated by adding an excess of NH_4PF_6 (~20-fold) solved in water. The red solid was filtered off and washed with water and diethyl ether. Further purification could be obtained via diffusion crystallization from DMF and Et_2O, yielding 66.4 mg (0.06 mmol, 29%) as a red solid.

^{1}H NMR (500 MHz, DMSO) δ 10.18 (d, J = 5.3 Hz, 2H), 8.95 (d, J = 8.7 Hz, 2H), 8.82 (d, J = 8.8 Hz, 2H), 8.70 (d, J = 8.9 Hz, 2H), 8.57 (d, J = 7.7 Hz, 2H), 8.48 (d, J = 8.9 Hz, 2H), 8.27 (td, J = 7.8, 1.4 Hz, 2H), 8.04 (ddd, J = 7.3, 5.3, 1.1 Hz, 2H), 7.78 (d, J = 6.6 Hz, 4H), 6.88 (d, J = 6.6 Hz, 4H), 2.03 (s, 6H). HRMS/ESI (+): calcd. for $C_{41}H_{31}N_9O_2Ru$ 391.58166, found 391.58189 $[M\text{-}2PF_6]^{2+}$, calcd. for $C_{41}H_{30}N_9O_2Ru$ 782.15604, found 782.15666 $[M\text{-}H\text{-}2PF_6]^+$.

ASSOCIATED CONTENT

Supporting Information

The Supporting Information is available free of charge at https://pubs.acs.org/doi/10.1021/acs.inorgchem.1c01646.

Additional details regarding the experimental and theoretical methodology and NMR, HRMS, and UV−vis spectra as well as additional details regarding the pK_a determination and the electrochemical and photocatalytic experiments (PDF)

AUTHOR INFORMATION

Corresponding Authors

Leticia González − *Institute of Theoretical Chemistry, Faculty of Chemistry, University of Vienna, Vienna 1090, Austria;* orcid.org/0000-0001-5112-794X; Email: leticia.gonzalez@univie.ac.at

Sven Rau − *Institute of Inorganic Chemistry I, Ulm University, Ulm 89081, Germany;* orcid.org/0000-0001-9635-6009; Email: sven.rau@uni-ulm.de

Authors

Fabian L. Huber − *Institute of Inorganic Chemistry I, Ulm University, Ulm 89081, Germany*

Anna M. Wernbacher − *Institute of Theoretical Chemistry, Faculty of Chemistry, University of Vienna, Vienna 1090, Austria;* orcid.org/0000-0002-7837-8674

Daniel Perleth − *Institute of Inorganic Chemistry I, Ulm University, Ulm 89081, Germany*

Djawed Nauroozi − *Institute of Inorganic Chemistry I, Ulm University, Ulm 89081, Germany;* orcid.org/0000-0002-3516-4756

Complete contact information is available at: https://pubs.acs.org/10.1021/acs.inorgchem.1c01646

Author Contributions

§F.L.H. and A.M.W. contributed equally. F.L.H. performed the synthesis of the discussed compounds and designed and performed the photophysical and photocatalytical experiments. A.M.W. performed the theoretical investigations. D.P. assisted during the course of the synthesis and photophysical and photocatalytical experiments. D.N. performed the electrochemical experiments. S.R. and L.G. supervised the research.

The manuscript was written and reviewed by F.L.H., A.M.W., S.R., and L.G.

Funding

This research was funded by the Deutsche Forschungsgemeinschaft DFG as part of the collaborative research center TRR234 "CataLight" (364549901), projects A4, B2, C3, and the Austrian Science Fund (FWF), project I 3987.

Notes

The authors declare no competing financial interest.

■ ACKNOWLEDGMENTS

The help of Maximilian Sender and Ivan Trentin in designing the 3D printed holder (Figure S1) used during irradiation in catalytic runs is thankfully acknowledged. A.M.W. thanks Sebastian Mai for helpful discussions and suggestions. The Vienna Scientific Cluster is gratefully acknowledged for computational resources.

■ REFERENCES

(1) Lewis, N. S.; Nocera, D. G. Powering the Planet: Chemical Challenges in Solar Energy Utilization. *Proc. Natl. Acad. Sci. U. S. A.* 2006, 15729−15735, DOI: 10.1073/pnas.0603395103.
(2) Meyer, T. J. The Art of Splitting Water. *Nature* **2008**, *451*, 778−779.
(3) Roger, I.; Shipman, M. A.; Symes, M. D. Earth-Abundant Catalysts for Electrochemical and Photoelectrochemical Water Splitting. *Nat. Rev. Chem.* **2017**, *1*, No. 0003.
(4) Romain, S.; Vigara, L.; Llobet, A. Oxygen-Oxygen Bond Formation Pathways Promoted by Ruthenium Complexes. *Acc. Chem. Res.* **2009**, *42*, 1944−1953.
(5) Sala, X.; Romero, I.; Rodríguez, M.; Escriche, L.; Llobet, A. Molecular Catalysts That Oxidize Water to Dioxygen. *Angew. Chem., Int. Ed.* **2009**, *48*, 2842−2852.
(6) Duan, L.; Wang, L.; Li, F.; Li, F.; Sun, L. Highly Efficient Bioinspired Molecular Ru Water Oxidation Catalysts with Negatively Charged Backbone Ligands. *Acc. Chem. Res.* **2015**, *48*, 2084−2096.
(7) Fan, T.; Duan, L.; Huang, P.; Chen, H.; Daniel, Q.; Ahlquist, M. S. G.; Sun, L. The Ru-tpc Water Oxidation Catalyst and Beyond: Water Nucleophilic Attack Pathway versus Radical Coupling Pathway. *ACS Catal.* **2017**, *7*, 2956−2966.
(8) Kärkäs, M. D.; Verho, O.; Johnston, E. V.; Åkermark, B. Artificial Photosynthesis: Molecular Systems for Catalytic Water Oxidation. *Chem. Rev.* **2014**, *114*, 11863−12001.
(9) Duan, L.; Bozoglian, F.; Mandal, S.; Stewart, B.; Privalov, T.; Llobet, A.; Sun, L. A Molecular Ruthenium Catalyst with Water-Oxidation Activity Comparable to That of Photosystem II. *Nat. Chem.* **2012**, *4*, 418−423.
(10) Matheu, R.; Garrido-Barros, P.; Gil-Sepulcre, M.; Ertem, M. Z.; Sala, X.; Gimbert-Suriñach, C.; Llobet, A. The Development of Molecular Water Oxidation Catalysts. *Nat. Rev. Chem.* **2019**, *3*, 331−341.
(11) Tong, L.; Zong, R.; Zhou, R.; Kaveevivitchai, N.; Zhang, G.; Thummel, R. P. Ruthenium Catalysts for Water Oxidation Involving Tetradentate Polypyridine-Type Ligands. *Faraday Discuss.* **2015**, *185*, 87−104.
(12) Zong, R.; Thummel, R. P. 2,9-Di-(2′-Pyridyl)-1,10-Phenanthroline: A Tetradentate Ligand for Ru(II). *J. Am. Chem. Soc.* **2004**, *126*, 10800−10801.
(13) Zhang, G.; Zong, R.; Tseng, H.-W.; Thummel, R. P. Ru(II) Complexes of Tetradentate Ligands Related to 2,9-Di(Pyrid-2′-yl)-1,10-Phenanthroline. *Inorg. Chem.* **2008**, *47*, 990−998.
(14) Wu, Q.; Zheng, K.; Liao, S.; Ding, Y.; Li, Y.; Mei, W. Arene Ruthenium(II) Complexes as Low-Toxicity Inhibitor against the Proliferation, Migration, and Invasion of MDA-MB-231 Cells through Binding and Stabilizing *c-Myc* G-Quadruplex DNA. *Organometallics* **2016**, *35*, 317−326.
(15) Stumper, A.; Lämmle, M.; Mengele, A. K.; Sorsche, D.; Rau, S. One Scaffold, Many Possibilities - Copper(I)-Catalyzed Azide-Alkyne Cycloadditions, Strain-Promoted Azide-Alkyne Cycloadditions, and Maleimide-Thiol Coupling of Ruthenium(II) Polypyridyl Complexes. *Eur. J. Inorg. Chem.* **2018**, *2018*, 586−596.
(16) Clayden, J.; Greeves, N.; Warren, S. *Organic Chemistry*; Oxford University Press, 2001.
(17) Duan, L.; Fischer, A.; Xu, Y.; Sun, L. Isolated Seven-Coordinate Ru(IV) Dimer Complex with $[HOHOH]^-$ Bridging Ligand as an Intermediate for Catalytic Water Oxidation. *J. Am. Chem. Soc.* **2009**, *131*, 10397−10399.
(18) Plasser, F. TheoDORE: A Toolbox for a Detailed and Automated Analysis of Electronic Excited State Computations. *J. Chem. Phys.* **2020**, *152*, No. 084108.
(19) Plasser, F.; Wormit, M.; Dreuw, A. New Tools for the Systematic Analysis and Visualization of Electronic Excitations. I. Formalism. *J. Chem. Phys.* **2014**, *141*, No. 024106.
(20) Plasser, F. *TheoDORE: A package for theoretical density, orbital relaxation, and exciton analysis* http://theodore-qc.sourceforge.net (accessed Jun 9, 2020).
(21) Mai, S.; Plasser, F.; Dorn, J.; Fumanal, M.; Daniel, C.; González, L. Quantitative Wave Function Analysis for Excited States of Transition Metal Complexes. *Coord. Chem. Rev.* **2018**, *361*, 74−97.
(22) Okamura, M.; Yoshida, M.; Kuga, R.; Sakai, K.; Kondo, M.; Masaoka, S. A Mononuclear Ruthenium Complex Showing Multiple Proton-Coupled Electron Transfer toward Multi-Electron Transfer Reactions. *Dalton Trans.* **2012**, *41*, 13081−13089.
(23) Kirchhoff, J. R.; McMillin, D. R.; Marnot, P. A.; Sauvage, J. P. Photochemistry and Photophysics of Bis(Terpyridyl) Complexes of Ruthenium(II) in Fluid Solution. Evidence for the Formation of an η^2-Diphenylterpyridine Complex. *J. Am. Chem. Soc.* **1985**, *107*, 1138−1141.
(24) Campagna, S.; Puntoriero, F.; Nastasi, F.; Bergamini, G.; Balzani, V. Photochemistry and Photophysics of Coordination Compounds: Ruthenium. *Photochem. Photophys. Coord. Compd. I* **2007**, *280*, 117−214.
(25) Pannwitz, A.; Prescimone, A.; Wenger, O. S. Ruthenium(II)-Pyridylimidazole Complexes as Photoreductants and PCET Reagents. *Eur. J. Inorg. Chem.* **2017**, *2017*, 609−615.
(26) Pannwitz, A.; Wenger, O. S. Proton Coupled Electron Transfer from the Excited State of a Ruthenium(II) Pyridylimidazole Complex. *Phys. Chem. Chem. Phys.* **2016**, *18*, 11374−11382.
(27) Walba, H.; Isensee, R. W. Acidity Constants of Some Arylimidazoles and Their Cations. *J. Org. Chem.* **1961**, *26*, 2789−2791.
(28) Huber, F. L.; Amthor, S.; Schwarz, B.; Mizaikoff, B.; Streb, C.; Rau, S. Multi-Phase Real-Time Monitoring of Oxygen Evolution Enables *in Operando* Water Oxidation Catalysis Studies. *Sustainable Energy Fuels* **2018**, *2*, 1974−1978.
(29) Muckerman, J. T.; Kowalczyk, M.; Badiei, Y. M.; Polyansky, D. E.; Concepcion, J. J.; Zong, R.; Thummel, R. P.; Fujita, E. New Water Oxidation Chemistry of a Seven-Coordinate Ruthenium Complex with a Tetradentate Polypyridyl Ligand. *Inorg. Chem.* **2014**, *53*, 6904−6913.
(30) Pineda-Galvan, Y.; Ravari, A. K.; Shmakov, S.; Lifshits, L.; Kaveevivitchai, N.; Thummel, R.; Pushkar, Y. Detection of the Site Protected 7-Coordinate $Ru^V = O$ Species and Its Chemical Reactivity to Enable Catalytic Water Oxidation. *J. Catal.* **2019**, *375*, 1−7.
(31) Liu, Y.; Ng, S.-M.; Yiu, S.-M.; Lam, W. W. Y.; Wei, X.-G.; Lau, K.-C.; Lau, T.-C. Catalytic Water Oxidation by Ruthenium(II) Quaterpyridine (Qpy) Complexes: Evidence for Ruthenium(III) Qpy-N, N‴-Dioxide as the Real Catalysts. *Angew. Chem.* **2014**, *126*, 14696−14699.
(32) Rau, S.; Büttner, T.; Temme, C.; Ruben, M.; Görls, H.; Walther, D.; Duati, M.; Fanni, S.; Vos, J. G. A Bibenzimidazole-Containing Ruthenium(II) Complex Acting as a Cation-Driven Molecular Switch. *Inorg. Chem.* **2000**, *39*, 1621−1624.

(33) Duan, L.; Xu, Y.; Zhang, P.; Wang, M.; Sun, L. Visible Light-Driven Water Oxidation by a Molecular Ruthenium Catalyst in Homogeneous System. *Inorg. Chem.* **2010**, *49*, 209−215.
(34) Matheu, R.; Ertem, M. Z.; Benet-Buchholz, J.; Coronado, E.; Batista, V. S.; Sala, X.; Llobet, A. Intramolecular Proton Transfer Boosts Water Oxidation Catalyzed by a Ru Complex. *J. Am. Chem. Soc.* **2015**, *137*, 10786−10795.
(35) Imidazole moieties from histidine-like H332 directly bound to Manganese 1 of the OEC and H337 located in the second coordination sphere both affect catalytic activity through changes in the degree of protonation (a) Retegan, M.; Neese, F.; Pantazis, D. A. Convergence of QM/MM and Cluster Models for the Spectroscopic Properties of the Oxygen-Evolving Complex in Photosystem II. *J. Chem. Theory Comput.* **2013**, *9*, 3832−3842. (b) Askerka, M.; Brudvig, G. W.; Batista, V. S. The O_2-Evolving Complex of Photosystem II: Recent Insights from Quantum Mechanics/Molecular Mechanics (QM/MM), Extended X-Ray Absorption Fine Structure (EXAFS), and Femtosecond X-Ray Crystallography Data. *Acc. Chem. Res.* **2017**, *50*, 41−48.
(36) Theerasilp, M.; Crespy, D. Halochromic Polymer Nanosensors for Simple Visual Detection of Local pH in Coatings. *Nano Lett.* **2021**, *21*, 3604−3610.
(37) Chakraborty, S.; Nandi, S.; Bhattacharyya, K.; Mukherjee, S. Time Evolution of Local pH Around a Photo-Acid in Water and a Polymer Hydrogel: Time Resolved Fluorescence Spectroscopy of Pyranine. *ChemPhysChem* **2019**, *20*, 3221−3227.

https://doi.org/10.1021/acs.inorgchem.1c01646
Inorg. Chem. 2021, 60, 13299−13308